Published in final edited form as:
Sci Transl Med. 2014 July 9; 6(244): 244ra89. doi:10.1126/scitranslmed.3008065.

Cortical GABAergic excitation contributes to epileptic activities around human glioma

Johan Pallud[1,2,3], **Michel Le Van Quyen**[#1], **Franck Bielle**[#4], **Christophe Pellegrino**[#5,6], **Pascale Varlet**[7], **Noemie Cresto**[1], **Michel Baulac**[1,8], **Charles Duyckaerts**[4], **Nazim Kourdougli**[5,6], **Geneviève Chazal**[5,6], **Bertrand Devaux**[2,3], **Claudio Rivera**[5,6,9], **Richard Miles**[1], **Laurent Capelle**[1,10], and **Gilles Huberfeld**[1,4,8,11]

[1]Institut du Cerveau et de la Moelle Epinière, INSERM UMRS975, CNRS UMR7225, Université Pierre et Marie Curie (UPMC), Paris, France. [2]Service de Neurochirurgie, Centre Hospitalier Sainte-Anne, Paris, France [3]Université Paris Descartes, France [4]Service de Neuropathologie, Centre Hospitalo-Universitaire Pitié-Salpêtrière, Assistance Publique - Hôpitaux de Paris (AP-HP), Paris, France. [5]INMED, Parc Scientifique de Luminy, Marseille, France [6]Université de la Méditerranée, UMR S901 Aix-Marseille Université, Marseille, France [7]Service de Neuropathologie, Centre Hospitalier Sainte-Anne, Paris, France [8]Unité d'Epileptologie, Centre Hospitalo-Universitaire Pitié-Salpêtrière, Assistance Publique - Hôpitaux de Paris (AP-HP), Paris, France. [9]Neuroscience Center, University of Helsinki, Finland [10]Service de Neurochirurgie, Centre Hospitalo-Universitaire Pitié-Salpêtrière, Assistance Publique - Hôpitaux de Paris (AP-HP), Paris, France. [11]Département de Neurophysiologie, UPMC, Centre Hospitalo-Universitaire Pitié-Salpêtrière, Assistance Publique - Hôpitaux de Paris (AP-HP), Paris, France.

[#] These authors contributed equally to this work.

Abstract

Rationale—Diffuse brain gliomas induce seizures in a majority of patients. As in most epileptic disorders, excitatory glutamatergic mechanisms are involved in the generation of epileptic activities in the neocortex surrounding gliomas. However, chloride homeostasis is known to be perturbed in glial tumor cells. Thus the contribution of GABAergic mechanisms which depend on intracellular chloride and which are defective or pro-epileptic in other structural epilepsies merits closer study.

Objective—We studied in neocortical slices from the peritumoral security margin resected around human brain gliomas, the occurrence, networks, cells and signaling basis of epileptic activities.

Results—Postoperative glioma tissue from 69% of patients spontaneously generated interictal-like discharges. These events were synchronized, with a high frequency oscillation signature, in superficial layers of neocortex around glioma areas with tumor infiltration. Interictal-like events

Corresponding author: Gilles Huberfeld, Institut du Cerveau et de la Moelle épinière - INSERM UMRS 975 - CNRS UMR 7225 UPMC - CHU Pitié-Salpêtrière, 47-83 Bd de l'Hôpital - 75013 Paris - France, Tel: +33 (0)1 57 27 42 32, gilles.huberfeld@upmc.fr.

Competing interest
None.

Europe PMC Funders Author Manuscripts

depended on both glutamatergic transmission and on depolarizing GABAergic signaling. About 65% of pyramidal cells were depolarized by GABA released by interneurons. This effect was related to perturbations in Chloride homeostasis, due to changes in expression of chloride co-transporters: KCC2 was reduced and expression of NKCC1 increased. Ictal-like activities were initiated by convulsant stimuli exclusively in these epileptogenic areas.

Conclusions—Epileptic activities are sustained by excitatory effects of GABA in the peritumoral human neocortex, as in temporal lobe epilepsies. Glutamate and GABA signaling are involved in oncogenesis and chloride homeostasis is perturbed. These same factors, induce an imbalance between synaptic excitatory and inhibition underly epileptic discharges in tumor patients.

Introduction

World Health Organization (WHO) gliomas in adults are highly epileptogenic primary brain tumors. The incidence of epilepsy varies from 60-100% in low-grade and 25-60% in high-grade gliomas, with 10-25% of refractory seizures(1, 2). Epileptogenesis may be linked to tumor invasion processes since epileptic activities seem to arise from the neocortex surrounding gliomas (3-5) and glioma cell infiltration seems to promote growth and recurrence of tumors at sites around their core (6, 7).

Epileptic activity has often been linked to changes in the balance between excitatory and inhibitory synaptic signaling. Excessive excitation has been reported in glioma tissue. Recent data shows massive glutamate release(8) underlies both epileptic activity and contributes to neuronal death as tumors progress. Potassium (K^+) buffering(9, 10) and glutamate clearance(11-13) are both impaired in gliomas, resulting in elevated extracellular glutamate and K^+ levels in peritumoral neocortex(14-17). On the other hand, neuronal inhibition may be defective. In the neocortex surrounding a tumor, $GABA_A$ receptors are reduced(18), and inhibitory interneurons are lost as are inhibitory synapses with pyramidal neurons(5, 19, 20). Work on non-tumoral human epileptic tissue suggests that GABAergic synapses generate depolarizing effects which contribute to epileptic activities(21-24). $GABA_A$ receptor channels are mainly permeable to Chloride (Cl^-). If the driving force for Cl^- induces an inward current, a cell will be hyperpolarized. In contrast an outward flux of Cl^- depolarizes neurons and may result in a functional excitation. In mature neurons, Cl^- concentration is normally regulated at low intracellular levels, by extrusion via the K/Cl co-transporter 2 (KCC2), while Cl^- loading by the Na/K/2Cl co-transporter 1 (NKCC1) is reduced(25). Recent data on human tissue suggests Cl^- homeostasis is altered in gliomas. Cl^- concentrations are increased both in neurons(26, 27), loaded by NKCC1(26, 28, 29) highly expressed in peritumoral human neocortex(30) possibly underlying epileptogenic effects, and in migrating tumor cells(31, 32), contributing to oncologic processes. We therefore asked whether the effects of a defective Cl^- homeostasis on GABAergic signaling might be involved in epileptogenesis of human peritumoral neocortex.

Spontaneous interictal-like discharges (IIDs) were generated by the surrounding neocortex infiltrated by glioma cells but not in the tumor core in slices of human peritumoral neocortex or in control tissue. Both depolarizing actions of GABA related to a perturbed Cl^-

homeostasis, and glutamatergic signaling contributed to these events. Interneurons fired at the onset of IIDs while 65% of pyramidal cells fired later during IIDs. In these pyramidal cells the actions of GABA were depolarizing and correlated with the local tumoral infiltration. Ictal-like discharges (IDs) induced by convulsants in the same areas, were preceded and possibly initiated by pre-ictal discharges (PIDs). These findings suggest that depolarizing GABAergic signals and glutamate-mediated signals c*(*8*)* contribute to human glioma-related epileptogenesis Mechanisms of epileptiform activities in the peritumoral neocortex of gliomas resemble those involved in temporal lobe epilepsies*(*21, 22, 24*)*, pointing to a common feature of human epileptogenesis. Furthermore, epileptogenesis and oncogenesis are linked by a defect in Cl^- homeostasis in peritumoral neocortex infiltrated by glioma cells.

Results

Identification of a spontaneous interictal-like activity

81 slices were studied from 47 fresh selected brain tissue specimens obtained from the ‘security margin’, the neocortex that surrounds the macroscopic tumor, from 29 patients with supratentorial hemispheric diffuse low-grade (n=17) or high-grade (n=12) gliomas (Figure 1A)*(*33*)*. Spontaneous activity was recorded from 74/81 (91.4%) slices from 42/47 (89.4%) brain tissue specimens from 28/29 (96.6%) patients (Figure 1B). The activity included spontaneous IIDs, consisting of a field potential and multi-unit firing, in records from 36/81 slices (44.4%) from 25/47 tissues (53.2%) from 20/29 patients (69%). Multiunit discharges alone were recorded from the remaining 38/45 slices (84.4%). IIDs were more frequent in slices (n=32/66, 48.5%) from patients (n=17/22, 77.3%) with preoperative seizures than in those (n=4/11, 26.7%) from patients (n=2/7, 26.7%) without seizures (p=0.05) (Figure 1C).

Spatial distribution of interictal-like activity

We asked whether sites of IIDs generation were correlated with regions of tumor infiltration. Only infrequent multi-unit activity was recorded from control tissue (14 slices from 7 patients) obtained at distances of ~ 30 mm from image-defined abnormalities during surgical access to different tumors. Histopathological analysis revealed no tumor infiltration at this distance in tissues obtained from 4 patients with insular glioma (n=7 slices), 2 patients with fronto-callosal glioma (n=4 slices), and one with a mesial temporal glioma (n=3 slices) (Figure 1B, 1C). IIDs were generated most often at locations “outside” (26/43, 60.5%) rather than “inside” (10/38, 26.3%) tumor abnormalities defined by imaging (p=0.004) (Figure 1C). Similarly, IIDs were generated significantly more frequently in slices without (30/54, 55.6%) rather than with (6/27, 22.2%) macroscopic tumor infiltration (p=0.005) (Figure 1C). Interictal-like discharges were recorded more often in slices with high tumor infiltration (6/7, 85.7%) than with low tumor infiltration (2/7, 28.7%) and never in slices with a solid tumor mass (0/4, 0%) (p=0.005) (Figure 1C, 1D). The density of CD3- (p=0.852), CD20- (p=0.472) and CD68-positive cells (p=0.645) or Ki67-positive cells in neocortex (p=0.852) or in white matter (p=0.772) had no significant influence. Thus, IIDs are not generated in the tumor core but rather in regions of tumor infiltration surrounding neocortical gliomas.

Cortical organization and electrophysiological characteristics

IIDs consisted of field potential associated with bursts of multi-unit firing (Figure 2A). Their mean amplitude was 57.9±11.5 μV (range, 22.5-166.2), mean duration, from onset to peak, was 24.4±7.9 ms (range, 7.4-44), and they recurred with mean frequency of 0.9±0.7 Hz (range, 0.1-4.2) (n=9723 events; n=36 slices). High frequency oscillations (HFOs) were nested within IIDs in 40.7% of extracellular records (11/27 slices; n=9 patients). They occurred during 71.9% of IIDs and the mean dominant frequency was 251±69 Hz (range, 150-350) (Figure 2A). HFO were never recorded from control tissue or sites without IIDs (Figure 2B, 2C). HFOs thus tended to confirm the epileptic nature of IIDs(34).

IIDs were synchronous within 'vertical' column-like regions in 31/36 slices (Figure 2B). They were recorded at a mean maximal depth of 2.1±1.5 mm (range, 0.5-5, n=31 slices) from pia mater (Figure 2E). IIDs were initiated preferentially from layers 3/4 (28/31 slices), and typically propagated to superficial layers (Figure 2C, 2D). HFOs were restricted to layers 3/4 suggesting IIDs were generated locally. IIDs propagated from their initiation site to a mean lateral distance of 1.3±0.94 mm (range 1-5, n=22 slices) (Figure 2C, 2E). Multiple, partly overlapping, asynchronous IID foci were detected in 25/36 slices (Figure 2D). The mean distance between foci was 1.8±1.2 mm (range, 0.7-5, n=22 slices). Spatial patterns of IID initiation and spread were similar in adjacent slices from 10/30 brain tissue specimens.

Thus, IIDs are generated at multiple neocortical sites surrounding gliomas and are spatially restricted to superficial and mid neocortical layers.

Pharmacology and cellular basis of interictal-like activity

We next examined the role of glutamatergic and GABAergic signaling in the genesis of IIDs. The NMDA receptor antagonist DL-APV (50 μM; n=6) had no effect, but the AMPA receptor antagonist DNQX (20 μM, n=6) suppressed IIDs (Figure 3A left). IIDs were also reversibly suppressed by $GABA_A$ receptor antagonists picrotoxin (50 μM; n=6) or gabazine (10 μM; n=5) (Figure 3A right). These data indicate that both excitatory and inhibitory synapses are involved in IID generation.

Intracellular recordings were made from single pyramidal cells and interneurons to characterize the neuronal and synaptic network basis of IID generation and specifically to examine the role of depolarizing responses to GABA. The mean resting potential of recorded pyramidal cells (n=20) was −60.3±8.1 mV (range, −50.0 to −79.0) and mean input resistance was 44.2±15.8 MΩ (range, 30-68). Interneurons (n=2) were distinguished by a fast firing pattern and a short action potential duration(35). They fired for 39±7 ms (mean ± s.d; range, 22-199) before IID initiation at a mean frequency of 78±36 Hz (range, 34-142; n=32 events), and were always active during IIDs (Figure 3B). The behavior of pyramidal cells during IIDs was variable. Cells distant from foci (n=3) did not consistently receive synaptic events during IIDs. 17 cells were recorded within the IID area. At resting potential, 6 of these neurons (35.3%) received hyperpolarizing synaptic events during IIDs. The remaining 11/17 cells (64.7%) received depolarizing synaptic events and sometimes fired during IIDs. In contrast to interneurons they never discharged before the onset of the IID

field. The resting membrane potential (mean, −62.6±10.3 mV; range, −79.0 to −50.0) and the input resistance (mean, 47.0±19.1 MΩ; range, 30.0-68.0) of cells that displayed depolarizing synaptic events were similar to the resting membrane potential (mean, −58.8±4.6 mV; range, −68.0 to −56.0) and input resistance (mean, 40.1±14.1 MΩ; range, 30.0-50.0) of cells that were hyperpolarized (p=0.859 and p=0.800, respectively). The excitability of the two cell groups was also similar. Depolarizing pulses of 0.5 nA and duration 100 ms? induced action potentials at 6.9±9.0 Hz in 11 cells that fired during IIDs. Identical stimuli applied to neurons that did not fire during IIDs induced action potentials at 6.8±9.2 Hz (p=0.46). We next compared the timing of firing and synaptic events received by interneurons (n=2) and pyramidal cells (n=5) during IIDs (Figure 3C). Both interneurons consistently fired before IID onset and before pyramidal cell discharges. Depolarizing PSPs also tended to precede hyperpolarizing PSPs, suggesting that interneuron firing may have contributed to IID initiation. We tested this hypothesis using the mu-opiate receptor agonist DAGO (10 μM; n=5) to hyperpolarize interneurons and effectively remove them from the network. DAGO reversibly suppressed IIDs in all 5/5 cases (Figure 3D), reinforcing the interneurons' drive hypothesis.

Depolarizing responses to GABA during IIDs

Interneuron firing preceded IID onset and most pyramidal cells were depolarized during IIDs. We asked whether pyramidal cell depolarization could result from GABA release by measuring the reversal potential of PSPs impinging on pyramidal cells (n=15) during IIDs (Figure 4A). Two distinct behaviors were apparent (Figure 4B). In 6/15 pyramidal cells (40%), synaptic events reversed negative to resting potential with a mean driving force of 7.8±3.9 mV (range, 4 to 14) (mean reversal potential: −66.6±4.0 mV (range, −72 to −62.5)). In the remaining 9/15 cells (60%), synaptic events reversed at values depolarized from resting potential with a mean driving force of −13.4±10.4 mV (range, −28 to −6) (mean reversal potential: −49.1±10.8 mV (range, −40 to −73)). The mean resting potential of the depolarized and hyperpolarized subgroups of cells was not significantly different (−58.8±4.6 mV (n=6) and 62.5±10.0 mV (n=9) respectively; p=0.414). Thus, GABAergic signaling depolarized about 60% of pyramidal cells situated close to an IID focus, similar to the 65% of cells receiving a depolarizing PSP during IIDs.

Since IIDs were associated with depolarizing actions of GABA and were present in regions of tumoral infiltration, we asked whether the depolarizing effects of GABA were limited to zones of infiltration. In infiltrated tissues, 9 out of 11 recorded pyramidal cells were depolarized by GABA during IIDs. In contrast, depolarization was detected in only 4 out of 9 cells recorded from tissue with no macroscopic or histopathological evidence for infiltration (p=0.019) (Figure 4B). The proportion of cells depolarized by GABA was higher in WHO grade IV gliomas (n=7/7) than in grade III (n=4/7) or grade II (n=2/6) gliomas (p=0.015)*(33)*.

Changes in expression or function of molecules that regulate Cl^- homeostasis could account for depolarizing GABAergic effects and contribute to tumor infiltration. The K-Cl co-transporter NKCC1 is expressed at low levels in non juvenile tissue*(36)*, while Cl^- extrusion by the transporter KCC2, maintains low levels of internal Cl^- in mature tissues so assuring

hyperpolarizing effects of GABA*(37)*. We measured levels of both transporters in Western blot analyses of 24 brain tissue specimens obtained from the 'security margin' of 12 patients with supratentorial diffuse low-grade (n=5) or high-grade (n=7) gliomas and on control samples (4 patients, 4 brain tissue specimens) obtained during surgical access to deep-seated metastasis of carcinomas. NKCC1 protein expression was significantly increased in peritumoral tissue (170±24%) compared to control (100±17%) (p=0.02) (Figure 4D). NKCC1 expression by glioma cells*(*28, 29, 38*)*, might mask possible changes of the protein in neurons. We therefore correlated NKCC1 expression with glioma infiltration. There was no significant difference of NKCC1 expression in peritumoral tissues with high tumor infiltration (148±14%) and those with low tumor infiltration (131±26%) (p=0.332). An upregulation of NKCC1 seems likely to have epileptogenic actions. We tested this hypothesis using bumetanide at doses where it acts selectively to suppress NKCC1 function (8 μM). In 6 slices, bumetanide reversibly suppressed IIDs over a period of 50±10-min (range, 45-60min) presumably reflecting time taken to establish new steady-state Cl^- levels in neurons (Figure 4C).

Levels of intra-neuronal Cl^- mainly depend on an equilibrium between NKCC1 mediated Cl^- load and KCC2 mediated Cl^- extrusion. We found KCC2 protein was significantly decreased (62±17%) from control (100±13%: p=0.04) in western blot of peritumoral tissue (Figure 4D). We next examined neuronal expression of KCC2 by immunohistochemistry using a KCC2-specific antibody (Figure 4E). The number of KCC2 negative neurons was significantly higher in peritumoral neocortex (45±13.2%) than in control tissue (12±6.5%) (p=0.04). Furthermore, when KCC2 was detected in neurons of peritumoral neocortex, immunostaining tended to be cytoplasmic (38.6%) rather than membranous (15.8%) compared to a largely membranous (71.3%) rather than cytoplasmic (16.2%) expression in control neurons. Exclusively membrane KCC2 immunostaining was much lower in neurons of peritumoral neocortex (15.8±6.7%) than controls (71.3±4.2%) (p=0.01). These differences in neuronal expression site should reduce KCC2 functionality in peritumoral neurons.

Taken together, these data point to an impaired Cl^- homeostasis in epileptogenic neocortex surrounding a glioma. GABA depolarizes a majority of pyramidal cells, due to both a loss of KCC2 immunoexpression and an increase in NKCC1 expression.

Induction of ictal-like activity

Ictal-like discharges (IDs) were induced pharmacologically in peri-tumoral tissue. Combining two pro-convulsant stimuli: an increase of extracellular K^+ to 8 mM and a reduction of external Mg^{2+} to 0.25 mM*(24)* induced IDs in 7/19 slices (36.8%) where IIDs were generated (3/8 patients; 37.5%). Two ID patterns could be distinguished (Figure 5A). The first consisted in recurrent rhythmic bursts of frequency 2.9±0.9 Hz (range, 1.2-4.3; n=34 events). The second involved an initial fast, low voltage activity (mean duration, 0.8±0.1 s; range, 0.65-0.99; n=8 events) at 270±97 Hz (range, 118-410), which then evolved into rhythmic bursts. The mean duration of IDs was 34.1±17.7 s (range, 6.2-62.1). The transition from IIDs to IDs occurred over 34.0±10.2 min (range, 20-50 min., n=6 slices). IDs then recurred at interval 54.7±62.4 s (range, 7.5-397.0; n=86 events) in the continued

presence of pro-convulsants. Slices of control brain tissue (n=14) did not generate IDs in response to the same pro-epileptic stimuli: increasing extracellular K^+ to 8 mM alone (n=8 slices) or coupled to a reduction of external Mg^{2+} to 0.25 mM (n=6 slices).

Pre-ictal discharges emergence and dynamics

Pre-ictal discharges (PIDs) were recorded in 14/19 slices exposed to pro-convulsant stimuli. In 7/7 slices PIDs preceded IDs, and comparable large field potentials were detected in 7/12 slices that did not exhibit later IDs. PID amplitude increased during the transition to ictal discharges and PIDs occurred concurrently with IIDs during this transition (Figure 5B, 5C). At steady state (n=446 events from 5 slices), PID amplitude and duration were larger than those of IIDs (mean, 336±114 vs 58±11 μV, $p<0.001$; and 32.5±15.4 vs 22.4±11.2 ms, n=446 events, $p<0.001$), but frequencies were similar (0.9±0.6 vs 0.93±0.7 Hz, $p=0.727$). PID fields were recorded from column-like regions with a maximal amplitude in superficial layers (7/7 slices) at distances of 1.4±0.7 mm (range, 1-3; n=7 slices) from the pia mater. PIDs propagated laterally for distances up to 3.5±1.3 mm (range 1.5-5; n=9 slices) from their initiation site. PIDs were never induced by identical stimuli in slices of control tissue (n=14).

HFOs associated with PIDs differed from those nested in IIDs (Figure 5D). HFOs were detected in 91% of electrodes recording PIDs (11/12; n=3 patients) as opposed to ~40% for IIDs. HFOs occurred throughout PIDs, but were restricted to IID onset. The range of HFO frequencies associated with PIDs was wider than that for IIDs although mean dominant frequencies were similar (266±90 vs 251±69 Hz). These data suggest that IIDs and PIDs may result from distinct processes with different spatial and temporal characteristics.

We next compared the role of GABAergic signaling in PIDs and IDs. IDs and IIDs were reversibly suppressed by blocking $GABA_A$ receptors (picrotoxin 50 μM; n=4; gabazine 10 μM; n=3) over a mean 33±6.6-min period (range, 30-40). However, PIDs were not blocked by these $GABA_A$ receptor antagonists (application of 45-70 min; Figure 5E). The NKCC1 antagonist bumetanide,which should reinforce hyperpolarizing effects of GABA, also had distinct actions on IIDs and PIDs At 8 μM, bumetanide abolished IIDs and IDs within 45 min (n=4). Bumetanide did not affect PIDs was in records longer than 75 min.

We explored the dynamics of PIDs at IDs onset. Once IDs occurred in recurring fashion, each ID (n=34 events; n=7 slices) was preceded by 5±4 PIDs (range, 1-19) during 11.7±7.7 s (range, 3.5-36.9) at a frequency of 0.46±0.2 Hz (range, 0.07-0.69). When PIDs were generated at distinct foci, the transition to ID was associated with an increased synchrony and conduction speed between foci (n=12 events from 2 slices from 2 patients) (Figure 6).

These data indicate that the neocortex surrounding glioma generates two forms of synchronous epileptiform activities during the transition to IDs: IIDs depend on depolarizing GABA and glutamatergic signaling whereas GABAergic transmission does not contribute to PIDs. ID initiation IDs requires functional GABAergic signaling and involves depolarizing effects of GABA which could be related to Cl^- accumulation in pyramidal cells, induced by recurring, synchronous PIDs.

Discussion

We have shown that peritumoral neocortex infiltrated by glioma cells in slices of human tissue, generates spontaneous interictal discharges. They are initiated, often at multiple sites of infiltrated neocortex, rather than in the tumor core, but. They depend on both glutamatergic and GABAergic signaling. The onset of IIDs was preceded by interneuron firing. GABA depolarized most pyramidal cells in infiltrated tissues, reflecting changes in Cl^- homeostasis due to both a reduced KCC2 expression and increased NKCC1 expression. ?Exposed to convulsants, peritumoral tissue generates IDs preceded by PIDs. These three glioma-related epileptiform activities (IIDs, PIDs, IDs) were detected only recorded in epileptic tissues. Population and neuronal behaviors, pharmacology and dynamics of these epileptiform activities generated by peritumoral cortex were very similar to those of sclerotic, epileptic human temporal lobe in *(*21, 22, 24*)* suggesting a common basis of pathological activities in two distinct epilepsy syndromes.

This spontaneous population synchrony generated by tissue from adult patients with a glioma should be classed as epileptic for several reasons. 1) It is comparable to interictal epileptic activity recorded during glioma surgery*(*3-5*)*. The spatial restriction in vitro may explain the rare spikes recorded in scalp electroencephalograms. 2) Multiunit activity was recorded from almost all slices, while only about half of the tissues generated IIDs. IIDs were generated focally at similar sites in adjacent slices from the same brain tissue, pointing to specific mechanism and location. 3) IIDs were generated in superficial layers of neocortex*(*8, 39*)* and in multiple peritumoral foci*(*4, 5*)*, but never in control samples. 4) HFOs, linked to zones of active epileptogenesis*(*40, 41*)*, were nested in IIDs. 5) IDs were induced exclusively in slices that generated IIDs. Thus, the peritumoral neocortex around gliomas is a pivotal structure both for the genesis of epileptic activity and for infiltration by glioma cells, which defines the oncological prognosis*(*6, 7*)*. This link may explain both the anti-epileptic effects of oncological treatments*(*42-45*)*, and the increase in seizure frequency as tumors progress*(*46*)*.

Our data suggest interneuron firing preceded IIDs. The resulting depolarization of large numbers of pyramidal cells may contribute to IID initiation.. Activation of $GABA_A$ receptors induced a depolarization in ~60% of pyramidal cells of peritumoral neocortex, suggesting that Cl^- homeostasis was perturbed due to an excessive Cl^- load mediated by NKCC1. These data recall results from sclerotic non-tumoral human epileptic tissue*(*21, 22*)* and are coherent with molecular defects identified in peritumoral tissues*(*30*)*. Indeed, NKCC1 immunoreactivity is strongly increased in peritumoral neocortex. In neurons Cl^- homeostasis is altered, the reversal potential of GABA-evoked current depolarizes and the efficacy of GABAergic inhibition is reduced *(*30*)*. Our results point to a disequilibrium between an excitatory glutamatergic drive and an inhibitory GABAergic brake, but with an excitatory brake rather than an inefficient one. An increased glutamatergic drive*(*8, 14, 16, 17*)*, due to both an increased release from glioma cells via the system x_c^- cystine-glutamate transporter*(*9, 12*)* and impaired glutamate uptake by glial cells*(*11*)*, would not only contribute to synchrony but also to excitotoxicity*(*8, 12*)*. Conversely, GABAergic signaling in peritumoral tissue seems likely to differ from that in normal tissue and may favor oncogenesis. GABA regulates glioma cell proliferation*(*32*)* and the grade of malignancy is

correlated with $GABA_A$ receptor expression by glioma cells(31). Intracellular Cl^- levels in migrating and proliferating glioma cells may reach ~ 100 mM(26, 27). These high levels are actively maintained by the NKCC1 cotransporter(26, 29), strongly expressed by glioma cells(28, 30). Blockade of NKCC1 reduces tumor growth in animal models(29). NKCC1 upregulation in neurons has been shown in experimental gliomas and in gangliogliomas, human glioneuronal tumors (30, 47). Several mechanisms may contribute to NKCC1 upregulation in peritumoral neurons. 1) Extracellular hyperosmolarity(48) due to Cl^- and K^+ release by tumor cells may enhance neuronal NKCC1 expression (27, 49). 2) BDNF release by glioma cells(50, 51) reduces KCC2 expression(52) and so should weaken Cl^- extrusion and reduce hyperpolarizing GABA responses in neurons. 3) The activation of WNK kinases by EGFR-dependent signals may activate NKCC1 in both glioma cells and neurons(53, 54). We note that NKCC1 protein expression is more elevated in high-grade gliomas than in low-grade gliomas. 4) The neurogenesis of neurons sharing immature phenotypes in response to glioma development(55).

Altogether, these data point to a similar defect in Cl^- homeostasis and GABAergic signaling in two epileptic syndromes with distinct aetiologies, severities and disease durations: peritumoral cortical regions of human gliomas and sclerotic human temporal lobe(21, 22, 24). This defect, together with an excessive glutamatergic excitatory drive, may be a common feature of human epileptogenesis. Molecules that control Cl^- homeostasis may be useful therapeutic targets for both epileptogenesis and tumor infiltration.

Methods

Patients

All individuals (48 patients, 38 males, 10 females; mean, 38±10 year-old; range, 23-62) gave their informed written consent and the “Comité Consultatif National d’Ethique” approved our protocol. Brain tissue specimens (n=78 from 48 individuals) containing neocortex were obtained as part of the planned ‘security’ margin of neurosurgical resection surrounding the tumor core. The location of each specimen was recorded with real-time intraoperative ultrasonography(5). The location of each brain tissue specimen was defined as “inside” or “outside” areas of hypersignal on ultrasonography matching maximal visible tumor abnormalities on MRI(56, 57). Control samples (4 patients, 4 brain tissue specimens) were obtained during surgical access to deep-seated metastasis of carcinomas (2 lungs, 1 breast, 1 colorectal, no seizure history).

Tissue preparation

After surgery, tissue was transported in a cold, oxygenated solution containing 248 mM dsucrose; 26 mM $NaHCO_3$; 1 mM KCl; 1 mM $CaCl_2$; 10 mM $MgCl_2$; 10mM d-glucose equilibrated with 5% CO_2 in 95% O_2. Neocortical slices of thickness 400 μm were cut with a vibratome (HM650V, Microm) to include regions of tumor infiltration. They were maintained at 37°C, equilibrated with 5% CO_2 in 95% O_2, in an interface chamber and perfused with a solution containing 124 mM NaCl; 26 mM $NaHCO_3$; 4 mM KCl; 2 mM $MgCl_2$; 2 mM $CaCl_2$ and 10 mM d-glucose.

Picrotoxin (50 μM) and gabazine (10 μM) were used to block $GABA_A$ receptors. 6,7-dinitroquinoxaline-2,3-dione (DNQX; 20μM) and DL-2-Amino-5-phosphonopentanoic acid (D,L-APV; 50 μM) were used to block glutamatergic signaling. [3H][D-Ala2,N-Me-Phe4,Gly5-ol]enkephalin (DAGO, 20μM) was used to block opioid mu receptors. Low doses of bumetanide (8 μM) were used to block the NKCC1 transporter. Ictal-like activity was induced by reducing Mg^{2+} to 0.25 mM and increasing external K^+ to 8 mM*(24)*.

Recordings

Up to four tungsten electrodes etched to a tip diameter of ~5 μm were used for extracellular recording. Signals were amplified 1000x and filtered to pass frequencies of 0.1 Hz to 10 kHz (AM systems, 1700). Intracellular records were made with glass microelectrodes containing 2M KAc and beveled to a resistance of 50-100 MΩ. Signals were amplified with an Axoclamp 2B amplifier in current clamp mode*(22)*.

Intracellular and extracellular signals were digitized at 10 kHz with a 12-bit, 16-channel A-D converter (Digidata 1200A, Axon Instruments), monitored and saved to a PC with the program Axoscope (Axon Instruments).

Data analysis

Recordings were analyzed with Clampfit (Axon Instruments) and Neuroexplorer (Nex technologies). Extracellular records were processed to detect either action potentials or field events. Field potential events were detected using an “up-only” algorithm with user-defined threshold.

High-frequency oscillations between 80-450 Hz were automatically detected using similar procedures to those of Staba et al.*(58)*. A detection threshold was defined as 4 standard deviations above the mean fluctuations of the envelope signal. Oscillatory events were defined as possessing more than 4 oscillatory cycles and 3 local maxima in both original and filtered signals. Time-frequency analyses were made with a Gabor wavelet (9 cycles), implemented with a modulated Gaussian window. The dynamics of synchronization in extracellular signals at the transition to ictal-like discharges were computed from a normalized cross-covariance function between extracellular recordings (moving window: 1 sec, overlap: 200 ms).

Histopathological and immunophenotypical analysis

The glioma core was examined in different tissue from that used for electro-physiological recording to establish the type and grade of the tumor according to the 2007 WHO classification *(33)*. Tissue was fixed in paraformaldehyde 4 % in PBS for 48-72 h. Paraffin-embedded tissue sections (20μm) were stained by Hematoxylin-eosin or processed for immunohistochemistry. After deparaffinization and inhibition of endogenous peroxidase, sections were microwaved in a sodium citrate buffer pH=6 for KCC2 antigen retrieval. The following antibodies were used: anti CD3 (Ventana); anti CD20 L26 1/1000 (Dako); anti CD68 KP1 1/1000 (Dako); anti KCC2 1/2000 (gift from Kai Kaila); anti Ki67 1/50 (Dako); anti NeuN 1/500 (Chemicon). We compared tumoral and peritumoral areas using a cut off (10 or more tumor cells per high power field (HPF); x400, 0.2 mm^2) to distinguish regions

of tumor infiltration and regions containing isolated tumor cells. CD68 immunoreactive cells were counted per HPF and Ki67 immunoreactive cells were counted per 10 HPF. At least 100 neurons were counted to determine the pattern of KCC2 immunoexpression.

On histopathological examination, we defined areas with solid tumor mass, high tumor infiltration and low tumor infiltration by isolated glioma cells in 18 slices taken adjacent to a recorded slice (10 patients, 4 high-grade, 6 low-grade gliomas).

Western blotting

Human samples were extracted using RIPA buffer (NaCl 150mM ; triton X-100 1% ; Doc 0,5% ; SDS 0,1% ; Tris HCl 50mM pH 8,0) supplemented with a cocktail of protease and phosphatase inhibitors (Roche) on ice. Protein quantification was performed using a BCA kit reaction (Pierce) and optical densities measured with a plate reader (BMG Labtek) at 562 nm. 20µg of protein samples together with 3X Laemmli buffer were run on 4-15% precast acrylamide gel (Bio-Rad) at 100 volts then blotted on nitrocellulose membrane. Immunoblotting of NKCC1 (gift from Chris Lytle) and KCC2 (gift from Kai Kaila) was made over-night at 4°C and revealed with a horse-radish peroxidase-conjugated antibody for 2 hours at room temperature. Protein levels were normalized against beta III tubulin antibodies (Covance). Revelation was performed on a G-Box Chemi system (Syngene). Bands were quantified with gel plot ImageJ plugin (version 1.47, NCBI).

Fluorescence quantification

Fluorescence images were obtained with an HCX APO 63x glycerol objective of a confocal microscope (Leica TCS SP5) using identical microscope and camera settings. Analysis was done by investigators blind to experimental groups using ImageJ software (NCBI). Briefly total immunofluorescence was determined by surrounding the cell body using enlarged NeuN mask and measured using Image J software (version 1.47, NCBI)..

Statistics

The JMP 7.2 software (SAS Institute Inc, Cary, NC, USA) was used and results expressed as mean±SD with significance of $p<0.05$. Exact p values are given unless $p<0.001$. Comparisons among groups were performed using Chi-square or Fisher's exact tests for categorical variables and using the nonparametric Mann-Whitney rank sum test for continuous variables. Relationships between variables were calculated using Spearman's rank order correlation.

Acknowledgements

We wish to thank Liset Menendez de la Prida, Severine Mahon and Stéphane Charpier for critical reading of the manuscript. We are grateful to Karima Mokthari, Clovis Adam, Marie-Joseph Madie and to the staff of the Service de Neuropathologie for the excellent technical assistance. We also thank Carine Karachi, Philippe Page, Fabrice Chrétien, Catherine Oppenheim, Jean-François Meder and Edouard Dezamis for their neurosurgical, neuroimaging and neuropathological contributions.

This work was funded by grants from the Institut National de la Santé Et de la Recherche Médicale (INSERM), the Centre National pour la Recherche Scientifique (CNRS), the Assistance Publique – Hopitaux de Paris (APHP), the Fédération pour la Recherche sur le Cerveau (FRC).

Financial Disclosure

None.

Abbreviations

DAGO	[3H][D-Ala2,N-Me-Phe4,Gly5-ol]enkephalin
D,L-APV	DL-2-Amino-5-phosphonopentanoic acid
DNQX	6,7-dinitroquinoxaline-2,3-dione
HFO	High frequency oscillation
ID	Ictal-like discharge
IID	Interictal-like discharge
IPSP	Inhibitory postsynaptic potential
KCC2	K/Cl co-transporter 2
NKCC1	Na/K/2Cl co-transporter 1
PID	Pre-ictal discharge
PSP	postsynaptic potential
WHO	World Health Organization

References

1. van Breemen MSM, Wilms EB, Vecht CJ. Epilepsy in patients with brain tumours: epidemiology, mechanisms, and management. Lancet neurology. 2007; 6:421–430.
2. Pallud J, Capelle L, Huberfeld G. Tumoral epilepsy. How does it happen? Epilepsia. 2013
3. Hirsch JF, Buisson-Ferey J, Sachs M, Hirsch JC, Scherrer J. [Electrocorticogram and unitary activites with expanding lesions in man]. Electroencephalogr Clin Neurophysiol. 1966; 21:417–428. [PubMed: 4162773]
4. Berger MS, Ghatan S, Haglund MM, Dobbins J, Ojemann GA. Low-grade gliomas associated with intractable epilepsy: seizure outcome utilizing electrocorticography during tumor resection. Journal of Neurosurgery. 1993; 79:62–69. [PubMed: 8315470]
5. Haglund MM, Berger MS, Kunkel DD, Franck JE, Ghatan S, Ojemann GA. Changes in gamma-aminobutyric acid and somatostatin in epileptic cortex associated with low-grade gliomas. Journal of Neurosurgery. 1992; 77:209–216. [PubMed: 1352540]
6. Pallud J, Varlet P, Devaux B, Geha S, Badoual M, Deroulers C, Page P, Dezamis E, Daumas-Duport C, Roux F-X. Diffuse low-grade oligodendrogliomas extend beyond MRI-defined abnormalities. Neurology. 2010; 74:1724–1731. [PubMed: 20498440]
7. Pallud, J. Springer Netherlands, Dordrecht: 2011. p. 153-161.
8. Buckingham SC, Campbell SL, Haas BR, Montana V, Robel S, Ogunrinu T, Sontheimer H. Glutamate release by primary brain tumors induces epileptic activity. Nat Med. 2011 doi: 10.1038/nm.2453.
9. Bordey A, Sontheimer H. Electrophysiological properties of human astrocytic tumor cells In situ: enigma of spiking glial cells. Journal of Neurophysiology. 1998; 79:2782–2793. [PubMed: 9582244]
10. Olsen ML, Sontheimer H. Functional implications for Kir4.1 channels in glial biology: from K+ buffering to cell differentiation. Journal of Neurochemistry. 2008; 107:589–601. [PubMed: 18691387]
11. Ye ZC, Rothstein JD, Sontheimer H. Compromised glutamate transport in human glioma cells: reduction-mislocalization of sodium-dependent glutamate transporters and enhanced activity of

Europe PMC Funders Author Manuscripts

cystine-glutamate exchange. Journal of Neuroscience. 1999; 19:10767–10777. [PubMed: 10594060]

12. De Groot J, Sontheimer H. Glutamate and the biology of gliomas. Glia. 2011; 59:1181–1189. [PubMed: 21192095]
13. Takano T, Lin JH, Arcuino G, Gao Q, Yang J, Nedergaard M. Glutamate release promotes growth of malignant gliomas. Nat Med. 2001; 7:1010–1015. [PubMed: 11533703]
14. Hamberger A, Nyström B, Larsson S, Silfvenius H, Nordborg C. Amino acids in the neuronal microenvironment of focal human epileptic lesions. Epilepsy Research. 1991; 9:32–43. [PubMed: 1909237]
15. Lyons SA, Chung WJ, Weaver AK, Ogunrinu T, Sontheimer H. Autocrine glutamate signaling promotes glioma cell invasion. Cancer Res. 2007; 67:9463–9471. [PubMed: 17909056]
16. Marcus HJ, Carpenter KLH, Price SJ, Hutchinson PJ. In vivo assessment of high-grade glioma biochemistry using microdialysis: a study of energy-related molecules, growth factors and cytokines. J Neurooncol. 2010; 97:11–23. [PubMed: 19714445]
17. Roslin M, Henriksson R, Bergström P, Ungerstedt U, Bergenheim AT. Baseline levels of glucose metabolites, glutamate and glycerol in malignant glioma assessed by stereotactic microdialysis. J Neurooncol. 2003; 61:151–160. [PubMed: 12622454]
18. Wolf HK, Roos D, Blümcke I, Pietsch T, Wiestler OD. Perilesional neurochemical changes in focal epilepsies. Acta Neuropathol. 1996; 91:376–384. [PubMed: 8928614]
19. Marco P, Sola RG, Ramón y Cajal S, DeFelipe J. Loss of inhibitory synapses on the soma and axon initial segment of pyramidal cells in human epileptic peritumoural neocortex: implications for epilepsy. Brain Res Bull. 1997; 44:47–66. [PubMed: 9288831]
20. Schaller B, Rüegg SJ. Brain tumor and seizures: pathophysiology and its implications for treatment revisited. Epilepsia. 2003; 44:1223–1232. [PubMed: 12919395]
21. Cohen I, Navarro V, Clemenceau S, Baulac M, Miles R. On the origin of interictal activity in human temporal lobe epilepsy in vitro. Science. 2002; 298:1418–1421. [PubMed: 12434059]
22. Huberfeld G, Wittner L, Clemenceau S, Baulac M, Kaila K, Miles R, Rivera C. Perturbed chloride homeostasis and GABAergic signaling in human temporal lobe epilepsy. J Neurosci. 2007; 27:9866–9873. [PubMed: 17855601]
23. Köhling R, Lücke A, Straub H, Speckmann EJ, Tuxhorn I, Wolf P, Pannek H, Oppel F. Spontaneous sharp waves in human neocortical slices excised from epileptic patients. Brain. 1998; 121(Pt 6):1073–1087. [PubMed: 9648543]
24. Huberfeld GG, de la Prida LLM, Pallud JJ, Cohen II, Le Van Quyen MM, Adam CC, Clemenceau SS, Baulac MM, Miles RR. Glutamatergic pre-ictal discharges emerge at the transition to seizure in human epilepsy. Nat Neurosci. 2011; 14:627–634. [PubMed: 21460834]
25. Miles R. Chloride Homeostasis and GABA. Signaling in Temporal Lobe Epilepsy. 2011:1–10.
26. Habela CW, Ernest NJ, Swindall AF, Sontheimer H. Chloride accumulation drives volume dynamics underlying cell proliferation and migration. Journal of Neurophysiology. 2009; 101:750–757. [PubMed: 19036868]
27. Habela CW, Olsen ML, Sontheimer H. ClC3 is a critical regulator of the cell cycle in normal and malignant glial cells. J Neurosci. 2008; 28:9205–9217. [PubMed: 18784301]
28. Ernest NJ, Sontheimer H. Extracellular glutamine is a critical modulator for regulatory volume increase in human glioma cells. Brain Res. 2007; 1144:231–238. [PubMed: 17320059]
29. Haas BR, Sontheimer H. Inhibition of the Sodium-Potassium-Chloride Cotransporter Isoform-1 reduces glioma invasion. Cancer Res. 2010; 70:5597–5606. [PubMed: 20570904]
30. Conti L, Palma E, Roseti C, Lauro C, Cipriani R, de Groot M, Aronica E, Limatola C. Anomalous levels of Cl(−) transporters cause a decrease of GABAergic inhibition in human peritumoral epileptic cortex. Epilepsia. 2011 doi:10.1111/j.1528-1167.2011.03111.x.
31. Labrakakis C, Patt S, Hartmann J, Kettenmann H. Functional GABA(A) receptors on human glioma cells. Eur J Neurosci. 1998; 10:231–238. [PubMed: 9753131]
32. Young SZ, Bordey A. GABA's control of stem and cancer cell proliferation in adult neural and peripheral niches. Physiology (Bethesda). 2009; 24:171–185. [PubMed: 19509127]
33. Louis DN, Carvenee WK. WHO classification of tumours of the central nervous system. 2007

34. Bragin A, Mody I, Wilson CL, Engel J. Local generation of fast ripples in epileptic brain. J Neurosci. 2002; 22:2012–2021. [PubMed: 11880532]
35. Menendez de la Prida L, Benavides-Piccione R, Sola R, Pozo MA. Electrophysiological properties of interneurons from intraoperative spiking areas of epileptic human temporal neocortex. Neuroreport. 2002; 13:1421–1425. [PubMed: 12167766]
36. Dzhala VI, Talos DM, Sdrulla DA, Brumback AC, Mathews GC, Benke TA, Delpire E, Jensen FE, Staley KJ. NKCC1 transporter facilitates seizures in the developing brain. Nat Med. 2005; 11:1205–1213. [PubMed: 16227993]
37. Rivera C, Voipio J, Payne JA, Ruusuvuori E, Lahtinen H, Lamsa K, Pirvola U, Saarma M, Kaila K. The K+/Cl− co-transporter KCC2 renders GABA hyperpolarizing during neuronal maturation. Nature. 1999; 397:251–255. [PubMed: 9930699]
38. Ernest NJ, Weaver AK, Van Duyn LB, Sontheimer HW. Relative contribution of chloride channels and transporters to regulatory volume decrease in human glioma cells. Am J Physiol, Cell Physiol. 2005; 288:C1451–60. [PubMed: 15659714]
39. Senner V, Köhling R, Püttmann-Cyrus S, Straub H, Paulus W, Speckmann E-J. A new neurophysiological/neuropathological ex vivo model localizes the origin of glioma-associated epileptogenesis in the invasion area. Acta Neuropathol. 2004; 107:1–7. [PubMed: 13680280]
40. Engel J, Bragin A, Staba R, Mody I. High-frequency oscillations: what is normal and what is not? Epilepsia. 2009; 50:598–604. [PubMed: 19055491]
41. Foffani G, Uzcategui YG, Gal B, Menendez de la Prida L. Reduced spike-timing reliability correlates with the emergence of fast ripples in the rat epileptic hippocampus. Neuron. 2007; 55:930–941. [PubMed: 17880896]
42. Zaatreh MM, Firlik KS, Spencer DD, Spencer SS. Temporal lobe tumoral epilepsy: characteristics and predictors of surgical outcome. Neurology. 2003; 61:636–641. [PubMed: 12963754]
43. Soffietti R, Baumert BG, Bello L, Von Deimling A, Duffau H, Frénay M, Grisold W, Grant R, Graus F, Hoang-Xuan K, Klein M, Melin B, Rees J, Siegal T, Smits A, Stupp R, Wick W. Guidelines on management of low-grade gliomas: report of an EFNS EANO* Task Force. Eur J Neurol. 2010; 17:1124–1133. [PubMed: 20718851]
44. Pace A, Vidiri A, Galiè E, Carosi M, Telera S, Cianciulli AM, Canalini P, Giannarelli D, Jandolo B, Carapella CM. Temozolomide chemotherapy for progressive low-grade glioma: clinical benefits and radiological response. Ann Oncol. 2003; 14:1722–1726. [PubMed: 14630675]
45. Sherman JH, Moldovan K, Yeoh HK, Starke RM, Pouratian N, Shaffrey ME, Schiff D. Impact of temozolomide chemotherapy on seizure frequency in patients with low-grade gliomas. Journal of Neurosurgery. 2011; 114:1617–1621. [PubMed: 21235313]
46. Rosati A, Tomassini A, Pollo B, Ambrosi C, Schwarz A, Padovani A, Bonetti B. Epilepsy in cerebral glioma: timing of appearance and histological correlations. J Neurooncol. 2009; 93:395–400. [PubMed: 19183850]
47. Aronica E, Boer K, Redeker S, Spliet WGM, van Rijen PC, Troost D, Gorter JA. Differential expression patterns of chloride transporters, Na+-K+-2Cl−-cotransporter and K+- Cl−-cotransporter, in epilepsy-associated malformations of cortical development. Neuroscience. 2007; 145:185–196. [PubMed: 17207578]
48. Kim JS, Kim WB, Kim Y-B, Lee Y, Kim YS, Shen F-Y, Lee SW, Park D, Choi H-J, Hur J, Park JJ, Han HC, Colwell CS, Cho Y-W, Kim YI. Chronic hyperosmotic stress converts GABAergic inhibition into excitation in vasopressin and oxytocin neurons in the rat. Journal of Neuroscience. 2011; 31:13312–13322. [PubMed: 21917814]
49. Buckingham SC, Robel S. Glutamate and tumor-associated epilepsy: Glial cell dysfunction in the peritumoral environment. NEUROCHEMISTRY INTERNATIONAL. 2013:1–6.
50. Yan Q, Yu H-L, Li J-T. [Study on the expression of BDNF in human gliomas]. Sichuan Da Xue Xue Bao Yi Xue Ban. 2009; 40:415–417. [PubMed: 19626994]
51. Chiaretti A, Aloe L, Antonelli A, Ruggiero A, Piastra M, Riccardi R, Tamburrini G, Di Rocco C. Neurotrophic factor expression in childhood low-grade astrocytomas and ependymomas. Child's nervous system : ChNS : official journal of the International Society for Pediatric Neurosurgery. 2004; 20:412–419.

52. Rivera C, Voipio J, Thomas-Crusells J, Li H, Emri Z, Sipilä S, Payne JA, Minichiello L, Saarma M, Kaila K. Mechanism of activity-dependent downregulation of the neuron-specific K-Cl cotransporter KCC2. Journal of Neuroscience. 2004; 24:4683–4691. [PubMed: 15140939]

53. Kahle KT, Rinehart J, Heros P. de Los, Louvi A, Meade P, Vazquez N, Hebert SC, Gamba G, Gimenez I, Lifton RP. WNK3 modulates transport of Cl− in and out of cells: implications for control of cell volume and neuronal excitability. Proc Natl Acad Sci USA. 2005; 102:16783–16788. [PubMed: 16275911]

54. Garzon-Muvdi T, Schiapparelli P, Ap Rhys C, Guerrero-Cazares H, Smith C, Kim D-H, Kone L, Farber H, Lee DY, An SS, Levchenko A, Quiñones-Hinojosa A. Regulation of brain tumor dispersal by NKCC1 through a novel role in focal adhesion regulation. PLoS Biol. 2012; 10:e1001320. [PubMed: 22570591]

55. Macas J, Ku M-C, Nern C, Xu Y, Bühler H, Remke M, Synowitz M, Franz K, Seifert V, Plate KH, Kettenmann H, Glass R, Momma S. Generation of neuronal progenitor cells in response to tumors in the human brain. Stem Cells. 2013 doi:10.1002/stem.1581.

56. Connor SEJ, Gunny R, Hampton T, O'gorman R. Magnetic resonance image registration and subtraction in the assessment of minor changes in low grade glioma volume. Eur Radiol. 2004; 14:2061–2066. [PubMed: 15252748]

57. Hammoud MA, Ligon BL, elSouki R, Shi WM, Schomer DF, Sawaya R. Use of intraoperative ultrasound for localizing tumors and determining the extent of resection: a comparative study with magnetic resonance imaging. Journal of Neurosurgery. 1996; 84:737–741. [PubMed: 8622145]

58. Staba RJ, Wilson CL, Bragin A, Fried I, Engel J. Quantitative analysis of high-frequency oscillations (80-500 Hz) recorded in human epileptic hippocampus and entorhinal cortex. Journal of Neurophysiology. 2002; 88:1743–1752. [PubMed: 12364503]

Tasks

JP, NC & GH performed the experiments

MLVQ, JP & GH analyzed electrophysiological data

FB, CP, PV, NK, GC & CD performed morphological and immunohistochemical analyses

MB, BD, CR, RM, LC, JP & GH contributed to design the experiments

LC & JP provided postoperative tissues

JP & GH wrote the ms

Europe PMC Funders Author Manuscripts

Europe PMC Funders Author Manuscripts

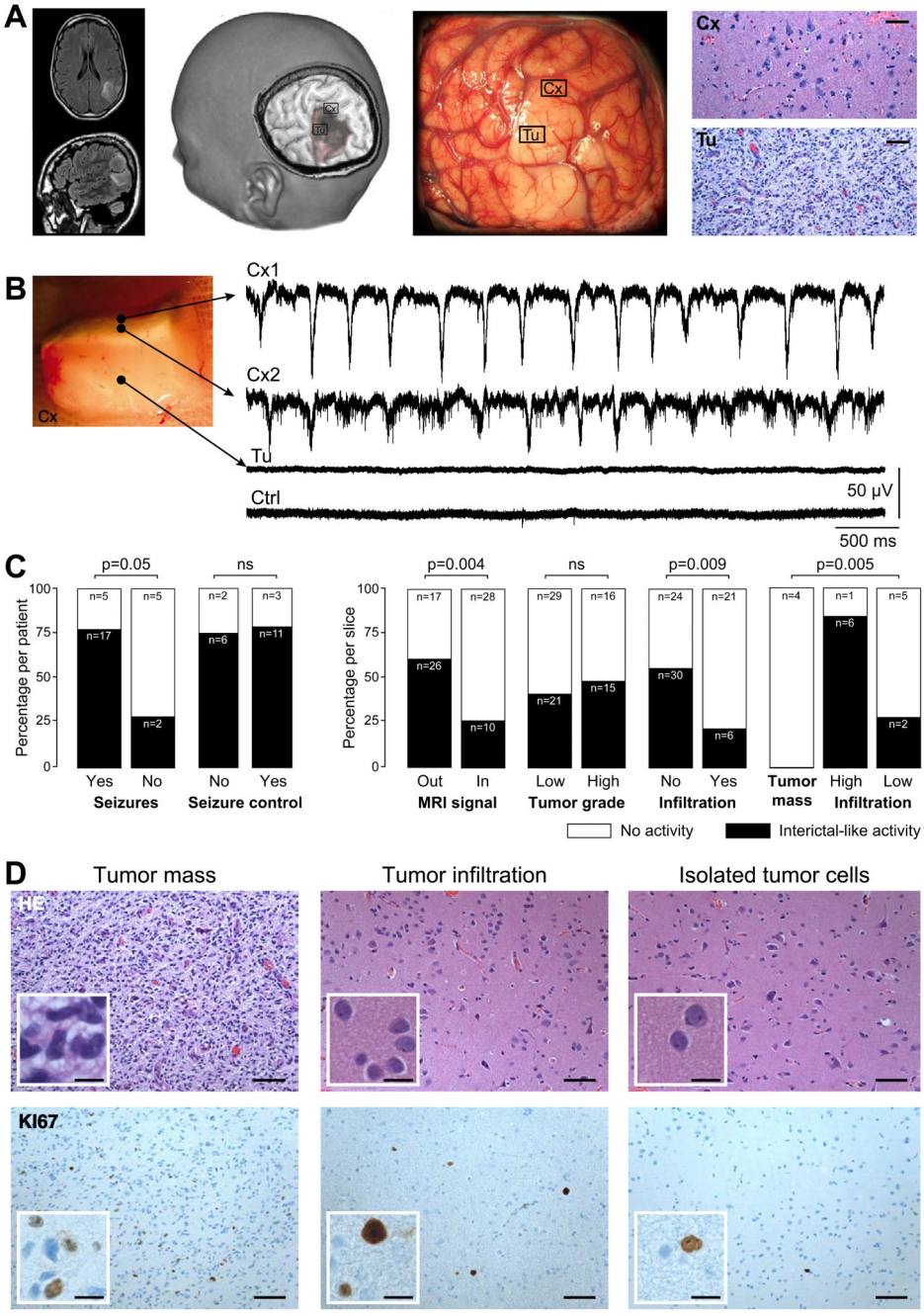

Figure 1. Interictal-like discharges are generated in the human neocortex infiltrated by glioma cells

(**A**) Example of a left parietal low-grade (World Health Organization grade II) glioma. The tumor appears as a hypersignal area on a Fluid Attenuated Inversion Recovery (FLAIR) sequence (left), as a hyposignal area on a three-dimensional spoiled gradient sequence (mid left) and as pale, hypertrophied and infiltrated, gyri on intraoperative photographs (mid right). Brain tissue specimens were sampled inside (Tu) and outside (Cx) macroscopic tumor infiltration. In areas outside visible tumor abnormalities (Cx) we detected only an infiltration by glioma cells (hematoxylin and eosin (HE) staining, x200). Tumor infiltration was

obvious in tissue from areas of visible imaging tumor abnormalities (Tu; HE staining, x200). Scale, 100 μm.

(**B**) Multiple extracellular recordings of interictal-like discharges (IIDs) from a slice containing both the solid tumor component and adjacent infiltrated neocortex. Electrode locations: Cx1, superficial neocortical layer; Cx2, mid neocortical layers, Tu, solid tumor tissue. Crtl shows a record from non-infiltrated neocortex in another control specimen.

(**C**) The proportion from which IIDs were (black) or were not (white) detected, compared to history of seizures (29 patients), preoperative seizures control with antiepileptic drugs (22 patients), position with respect to structural abnormalities (81 slices; inside Vs outside regions of FLAIR hypersignal on MRI), tumor grade (81 slices; low-grade Vs high-grade), tumor infiltration (81 slices Vs control 14 slices), and indices (18 slices) of tumor core (n=4), high tumor infiltration (n=7) or low tumor infiltration by isolated tumor cells (n=7) from histopathological analyses.

(**D**) Classical histolopathogical features of a glioma. The tumor mass (left), and regions with tumor infiltration (middle) and with isolated glioma cells (right) are shown with HE (upper) and Ki67 (lower) stains. Scales: 100 μm and 25 μm for the insets.

Europe PMC Funders Author Manuscripts

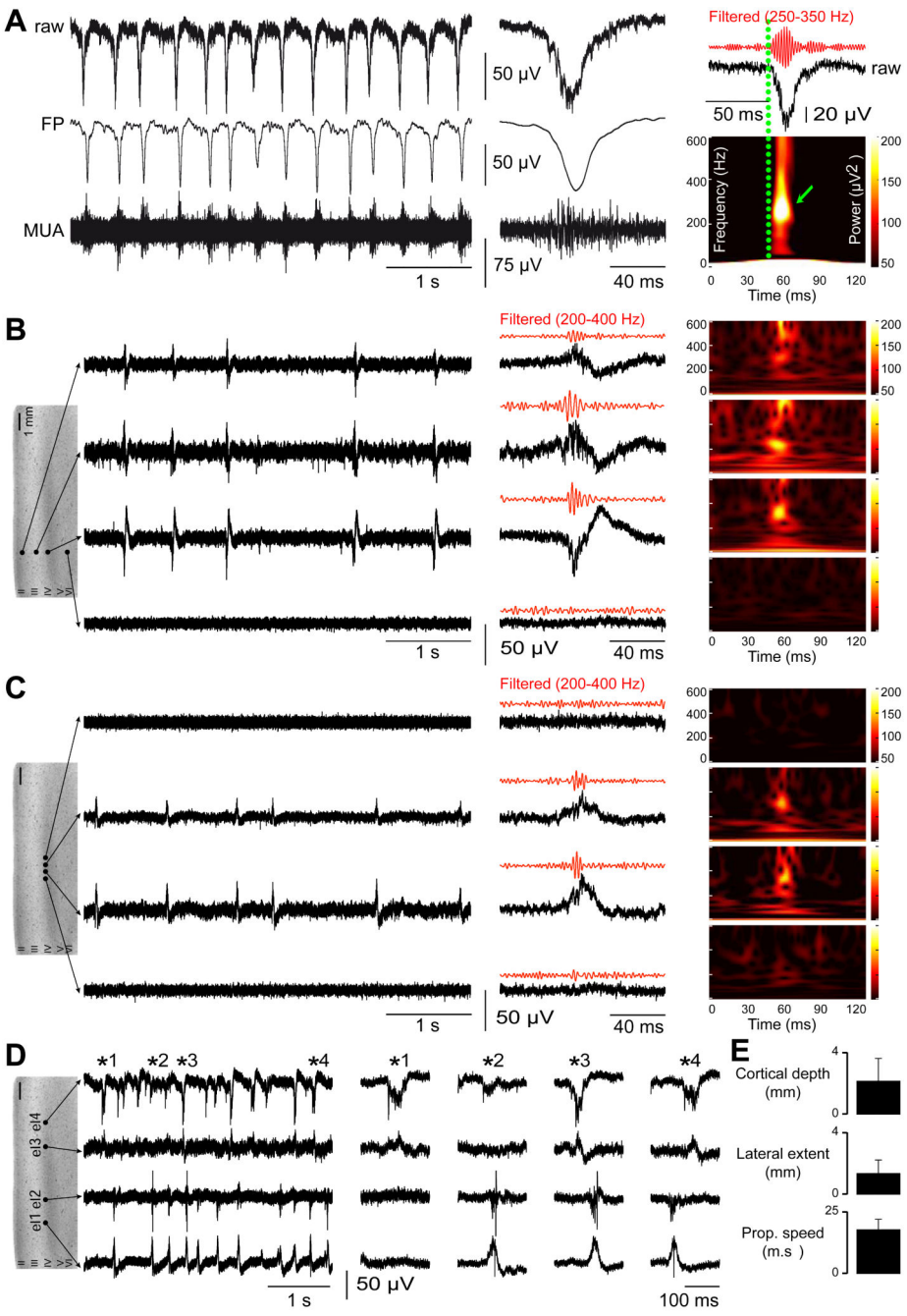

Figure 2. Interictal-like discharges are spatially restricted to superficial neocortical layers and are generated in multiple sites

(**A**) Extracellular records of interictal-like discharges (IIDs). They consist of bursts of multi-unit activity (MUA; > 300 Hz high pass filter) correlated with field potentials (FP, < 100 Hz low pass filter) (left). Expanded raw, MUA and FP traces at middle (middle). High frequency oscillations (HFOs; filtered to pass 250–350 Hz) are detected during IIDs (right). Time frequency plots (below) show a mean dominant frequency of 251±69 Hz (n=572 events).

(**B, C**) Multiple extracellular records of IIDs from slices containing infiltrated neocortex. In B, four electrodes are placed at different depths of the same neocortical column. They show IIDs and HFOs were synchronous in a vertical column-like region with field onset, maximal amplitude and the largest HFO in layers III-IV. In C, four electrodes are placed in layers IIIIV at the same depth over a lateral distance of 1 mm. They show a spatially restricted lateral spread of IIDs and HFOs. HFOs were never detected in the absence of IIDs.
(**D**) IIDs are initiated at multiple foci in infiltrated neocortex. Multiple records from a slice of infiltrated neocortex with four electrodes (el) located in layers III-IV at separations of: el1 – 1mm – el2 – 3mm – el3 – 1mm – el4. Expanded traces in the middle.
(**E**) Mean±SD of the neocortical depth, lateral extent and propagation speed of IIDs in the recorded slices.

Europe PMC Funders Author Manuscripts

Europe PMC Funders Author Manuscripts

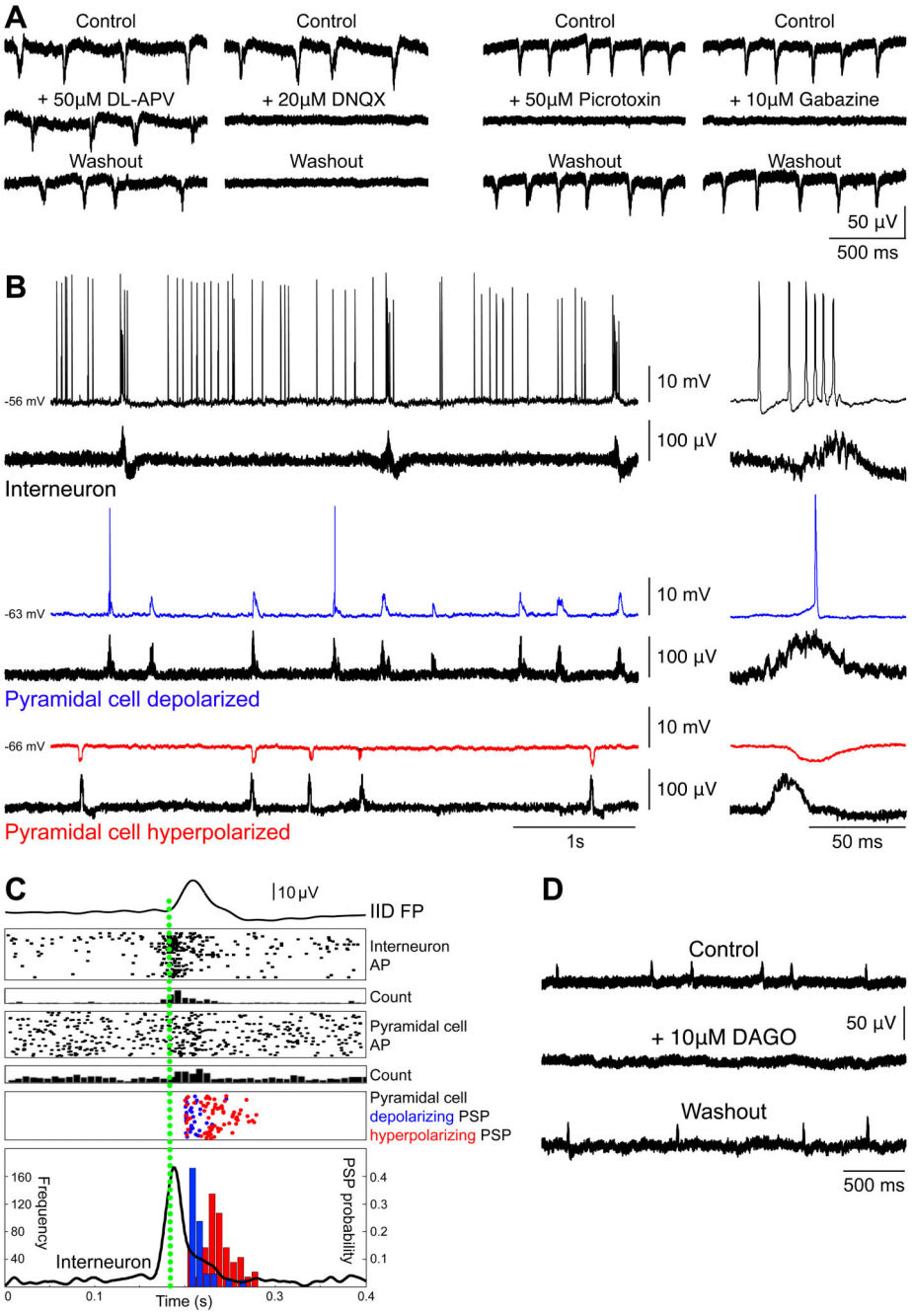

Figure 3. Interictal-like discharges pharmacology and cellular correlates

(**A**) Pharmacology of Interictal-like Discharges (IIDs). The NMDA receptor blocker D,L-APV (50 µM) did not modify extracellularly recorded IIDs, but they were suppressed by the AMPA receptor antagonist DNQX (20 µM) (left). The $GABA_A$ receptor antagonist Picrotoxin (50 µM) and gabazin (10 µM) reversibly blocked IIDs (right).

(**B**) Cellular basis of IIDs. Spontaneous intracellular (upper) and extracellular (lower) records of neurons from infiltrated neocortex. Expanded traces of a single IID at right. An

Europe PMC Funders Author Manuscripts

interneuron (top, black) fired before and during IID initiation. Some pyramidal cells were depolarized (middle, blue) others hyperpolarized during IIDs (bottom, red).
(**C**) Timing of cellular firing during IIDs. Mean population field activity (IID FP; top) plotted against sequential raster traces and peri-event histogram of interneuron firing (Interneuron AP, and count). Raster traces and peri-event histogram for firing of an excited pyramidal cell (Pyramidal cell AP and count). Timing of the peak of depolarizing (blue) and hyperpolarizing PSPs (red). The time course of interneuron firing (black line), and the probability of depolarizing (red) and hyperpolarizing PSPs (blue) are shown in the lower box.
(**D**) Hyperpolarizing interneurons with DAGO (10 μM), the opioid mu receptor agonist, reversibly suppressed IID field potentials.

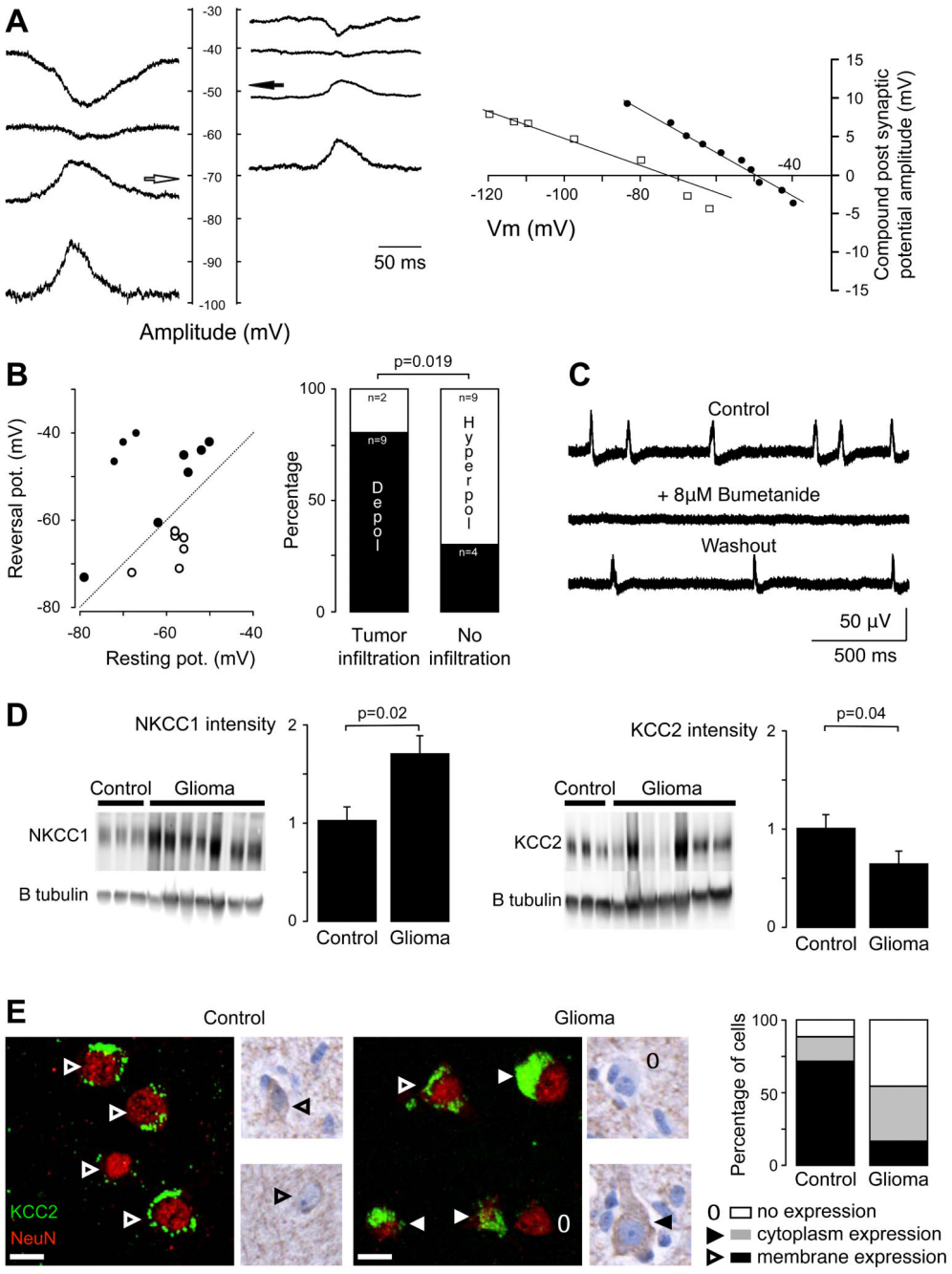

Figure 4. Cl^- regulation impairment contributes to interictal-like discharges

(**A**) $GABA_A$ reversal potential (Vrev) in pyramidal cells. PSP amplitude during interictal-like discharges (IIDs) was measured in pyramidal cells of infiltrated neocortex maintained at different potentials. Records are shown (at the left) and plotted (at right) from one cell with a Vrev of – 71 mV (white arrow and plotted open squares) and another cell with Vrev values of – 48 mV (black arrow and plotted filled circle).

(**B**) Correlation of Vrev and resting potential for 15 pyramidal cells. Reversal potentials were depolarizing with respect to rest in 9 cells (filled circles), above the diagonal line, and

hyperpolarizing in 6 cells (open circles) below the line. The proportion of pyramidal cells depolarized by GABA during IIDs (black part of the histogram- Depol vs white part - Hyperpol) was significantly higher in tissues with tumor infiltration than in tissues with no infiltration (p=0.019, Fisher exact test).

(C) Blocking the K-Cl cotransporter NKCC1 with bumetanide (8 μM) reversibly suppressed spontaneous IID field potentials.

(**D**) Western blot for NKCC1 (left) and KCC2 (right) of both control (n=4) and glioma (n=7) human tissues. All results were normalized using beta III tubulin neuronal-specific marker. Histogram representing normalized NKCC1 protein quantification shows that NKCC1 is significantly increased in glioma samples as compared to controls (p=0.02). Histogram representing normalized KCC2 protein quantification shows that KCC2 is significantly decreased in glioma samples as compared to controls (p=0.04).

(**E**) Illustrations of KCC2 immunoreactivity stained with NeuN marker. Left, the fluorescence is distributed along the plasma membrane (arrow head) of the cells in controls. Middle, in glioma sample, the distribution of KCC2 immunoreactivity in neurons of infiltrated neocortex is modified from membrane staining (open arrow head), staining in the cytoplasmic region (filled arrow head) to a loss of staining (open circle). Right, the quantification of KCC2 fluorescence repartition per cell shows a significant decrease of membrane staining (p=0.01) and a significant increase in the loss of staining in glioma samples (p=0.04), as compared to controls. Scale bar, 10 μm.

Europe PMC Funders Author Manuscripts

Europe PMC Funders Author Manuscripts

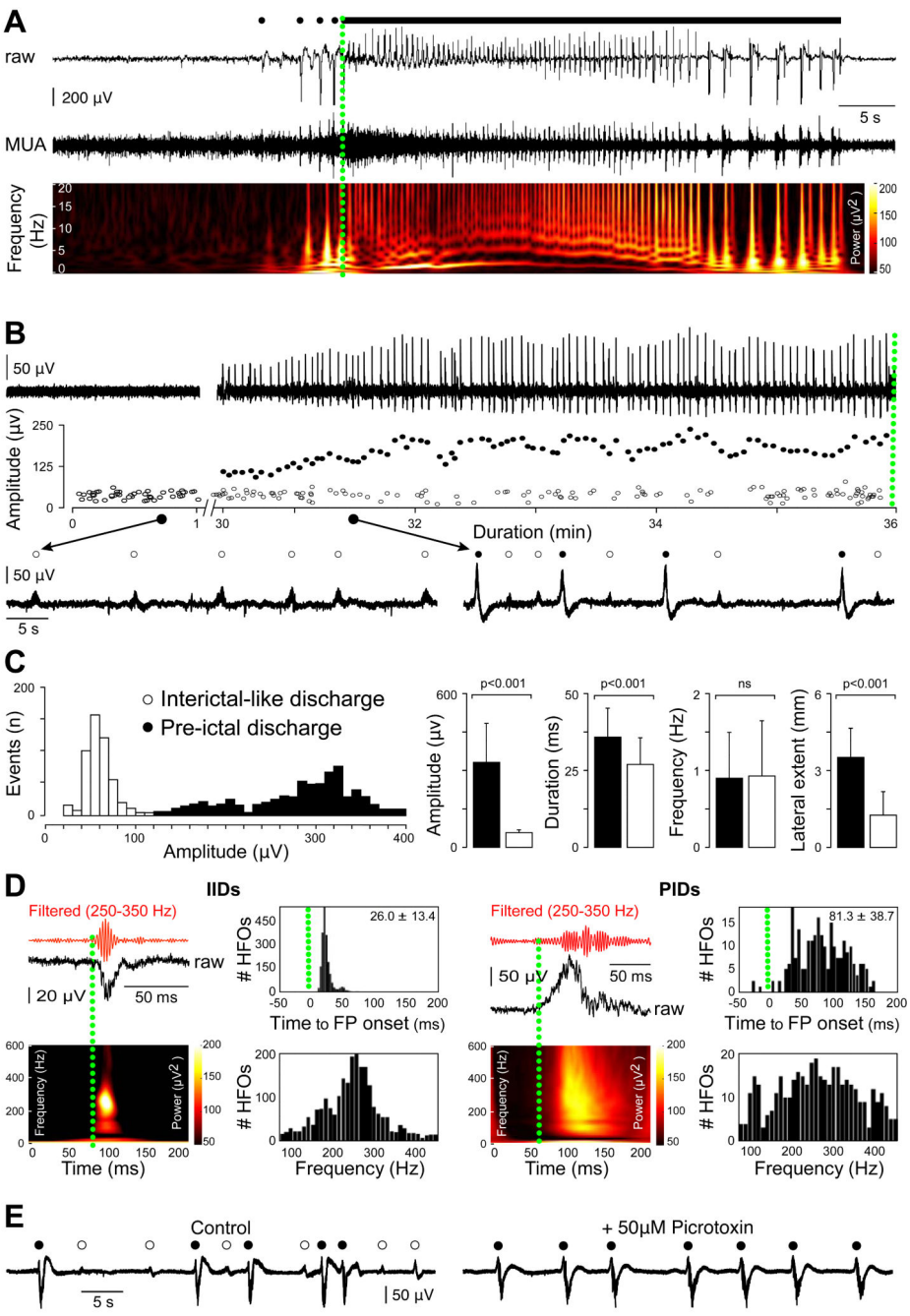

Figure 5. Ictal-like discharges generated in the human neocortex surrounding gliomas are preceded by a specific pre-ictal activity

(**A**) Extracellular records of an ictal-like discharge (ID) induced by exposure to 0.25 mM Mg^{2+} and 8 mM K^{+}. Pre-ictal discharges (PIDs, black filled circles) recurred before seizure onset followed by rhythmic bursts. Multi-unit activity (MUA) and time frequency plot of the local field potential (LFP).

(**B**) PIDs emerge during the transition to ictal-like activity in vitro. Extracellular records of the transition to ictal-like activity (0.25 mM Mg^{2+} and 8 mM K^{+}). Amplitudes of field potentials during the transition show the emergence of larger PIDs, while amplitudes of

Europe PMC Funders Author Manuscripts

interictal-like discharges (IIDs, open circles) did not change. Below: IIDs before convulsant application (left) and co-occurrence of PIDs and IIDs during the transition (right).
(**C**) Differences in IID and PID field potentials. Amplitude distributions of all field potentials during the transition distinguish between IIDs and PIDs. Mean±SD of the amplitude, duration, frequency and lateral extent, of IIDs (white) and PIDs (black) at steady state. The amplitude, duration and lateral extent, but not frequency, were significantly different.
(**D**) High frequency oscillations (HFO) occurring during IIDs (left, n=284 events) and PIDs (right, n=294 events). For each type of activity: top left: HFO recording (red trace) during a FP (black trace); bottom left HFO time frequency representation; top right: histogram of HFOs timing with respect to a population event (the mean frequency ±sd is indicated); bottom right: histogram of HFO frequency distribution during population event. Population FP onset is shown as a green dotted line. HFOs associated with IIDs possessed a narrow frequency spectrum and were restricted to the onset of an IID. HFOs during PIDs spanned the frequency spectrum and persisted throughout PIDs.
(**E**) IIDs do not depend on GABAergic signaling. Extracellular record of IIDs and PIDs at steady state in a 0.25 mM Mg^{2+} and 8 mM K^{+} solution. The $GABA_A$ receptor antagonist picrotoxin (50 μM, for 30 min) reversibly blocked IIDs, but not PIDs

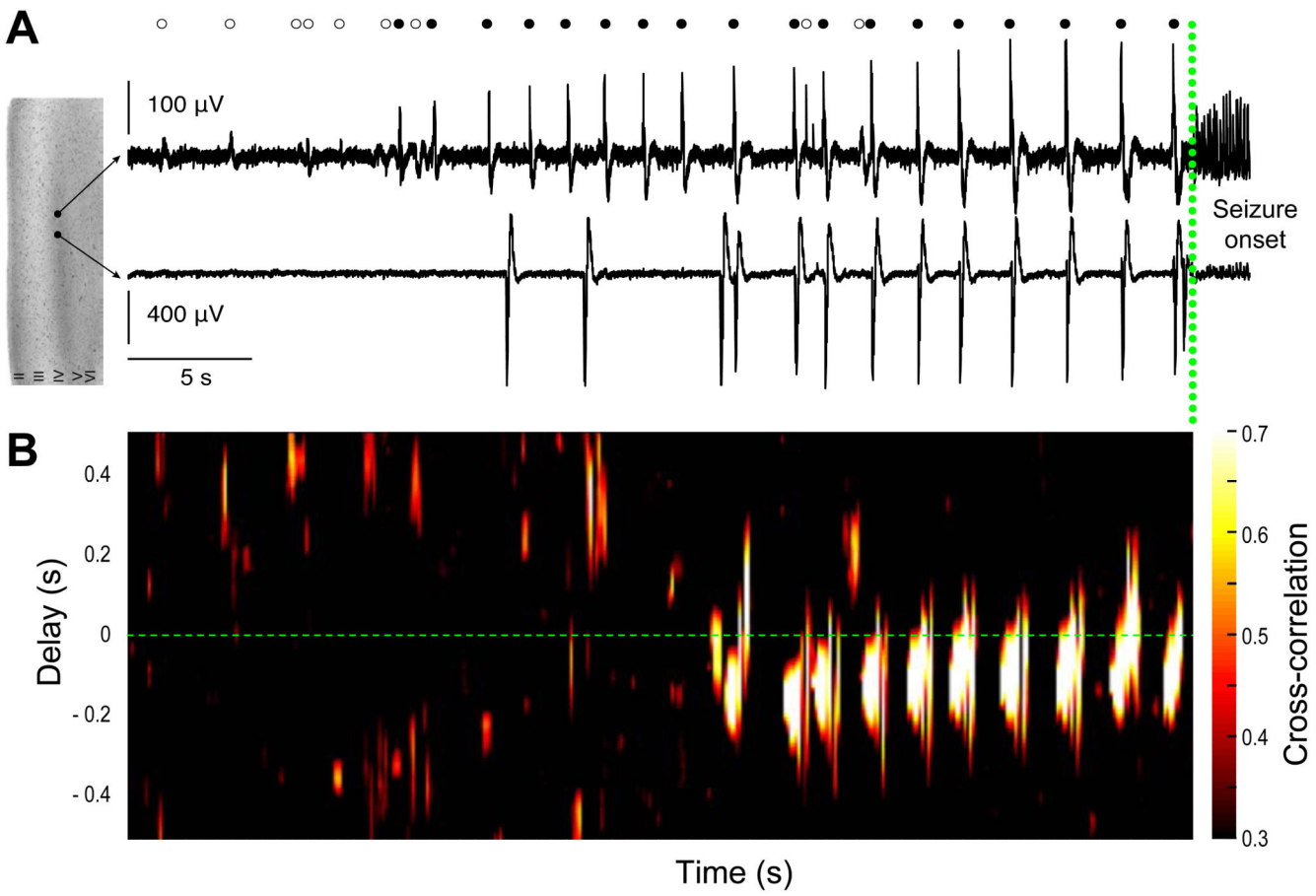

Figure 6. Dynamics of population activity at the initiation of ictal-like events

(**A**) Dual extracellular records during the initiation of a seizure-like event with seizure onset shown by a green dotted line. Interictal-like discharges (IIDs, open circles) and pre-ictal discharges (PIDs, filled circles) during the transition are shown above. PIDs are progressively recruited and recur before seizure onset.

(**B**) Time delay and cross correlation of PIDs initiated at two distinct foci recorded by two electrodes. During seizure initiation, synchrony increased progressively and propagation delay between the two PID foci was reduced.

Europe PMC Funders Author Manuscripts